CHEMPLUSCHEM

DOI: 10.1002/cplu.201100051

Facile and Low-Cost Synthesis of Large-Area Pure V_2O_5 Nanosheets for High-Capacity and High-Rate Lithium Storage over a Wide Temperature Range

Zhong-li Wang, Dan Xu, Li-min Wang, and Xin-bo Zhang*[a]

One of the great challenges in the development of next-generation lithium ion batteries is to simultaneously achieve high power and large energy capacity. Herein, large-area pure V_2O_5 nanosheets are successfully synthesized by a novel and facile dissolution–splitting method using low-cost raw materials. The as-prepared product exhibits enhanced lithium storage properties including high reversible capacity (290 mAh g^{-1}), good cycling and rate performance (144 mAh g^{-1} at 10 C and 95 mAh g^{-1} at 20 C), which can deliver a high power density of 15.6 kW kg^{-1} while the energy density remains as high as 260 Wh kg^{-1}. At low temperatures of 0 and −20 °C, the V_2O_5 nanosheets can still deliver high capacities of 184 and 158 mAh g^{-1} at 1 C, respectively, and also exhibit excellent cycling stability.

Introduction

The rapid development in next-generation portable electronic devices and the ever-increasing interest in plug-in hybrid electric vehicles (PHEVs) urgently demand a further increase in the energy and power capabilities of lithium ion batteries (LIBs). However, even after decades of intensive efforts, the low capacity of the current electrode materials, especially at the cathode side, still limits improvement of power and energy density of LIBs. For use as a versatile power source, it is still a challenge to simultaneously achieve high capacity and high rate performance of the cathode materials.

Enhancements in capacity necessarily require transformation from the present Li insertion/deinsertion compounds limited by $1e^-$ per formula unit into novel and advanced compounds based on multielectron reaction materials. However, the present multielectron systems such as metal vanadates and metal fluorides suffer from bad cycling stability and low rate performance.[1–3] On the other hand, in achieving a high power density, rapid ionic and electronic diffusion in electrode materials are necessary. Recently, many strategies, such as decreasing the electrode materials to the nanoscale size, coating or mixing with more conductive materials, and doping of electrode materials with foreign atoms, have been developed to improve the power density.[4–6] In particular, an ultrafast discharge rate as high as 400 C was achieved by Kang and Ceder.[4] Although much progress has been made, there are still some problems such as poor cycling stability and the requirement of a high percentage of carbon black. Therefore, there is an impending need to improve the performance of LIBs to simultaneously hold high power and large energy capacity.

Vanadium pentoxide is important among a family of functional inorganic materials, and has numerous applications in the field of catalysis,[7] chemical sensors,[8] and electric field-effect transistors[9] as well as multielectron battery materials. Since the reversible multielectron electrochemical lithium ion intercalation in V_2O_5 was first reported in 1976 by Whittingham,[10] intense interest has been focus on applying vanadium pentoxide as a cathode material for rechargeable LIBs because of its high theoretical capacity, low cost, and abundance.[11–20] Unfortunately, so far its practical application in rechargeable LIBs is still seriously hindered by the poor cycle stability, low electronic and ionic conductivity, and sluggish electrochemical kinetics.[13] Two-dimensional (2D) structure of nanosheets (NSs) have received increased interest for their application in energy-harvesting devices.[21,22] 2D material-based LIBs could offer significant improvements in power and energy density over bulk electrodes stemming from the following advantages: 1) the facile strain relaxation of the large-area 2D structure can greatly improve the structural stability against volume expansion and thus would theoretically benefit the cycling stability. 2) The large surface to volume ratio of the 2D geometry offers a sufficient contact interface with the electrolyte and the thin structure shortens the ion and electron transport length, which would effectively maximize electron and Li^+ ion diffusion and thus could allow ultrafast lithium storage. In this context, 2D nanosheets of metal oxides such as TiO_2 and SnO_2 have been shown to exhibit superior lithium storage properties.[21,22] However, the synthesis and lithium storage properties of large-area thin V_2O_5 NSs enabling stable and fast multielectron reaction have not been investigated.

Layered materials represent a diverse and largely untapped source of 2D systems and provide wide selections of nanosheet crystallites. Inspired by the great success in exfoliation of

[a] Dr. Z.-l. Wang, Dr. D. Xu, Prof. L.-m. Wang, Prof. Dr. X.-b. Zhang
State Key Laboratory of Rare Earth Resource Utilization
Changchun Institute of Applied Chemistry, Chinese Academy of Sciences
Changchun, 130022 (P. R. China)
E-mail: xbzhang@ciac.jl.cn

Supporting information for this article is available on the WWW under http://dx.doi.org/10.1002/cplu.201100051.

layered graphite to graphene, metal oxide NSs might also be synthesized by disintegrating a layered compound into the constituent single or few layers. Up to now, transition-metal oxide NSs such as $Ca_2Nb_3O_{10}$, Nb_6O_{17}, $Ti_{1-\delta}O$, and MnO_2 have been prepared by exfoliation from their layered bulk counterparts.[23–26] The traditional synthesis of metal oxide NSs often requires multistep processing, which involves a high-temperature solid-state reaction, protonation of interlayer alkali metal ions, and an acid–base reaction with an aqueous solution of quaternary ammonium cations.[27] However, when such a method was applied to synthesize V_2O_5 NSs, it was found that V_2O_5 was easily dissolved by the swelling agent (e.g. terabutylammonium hydroxide) because V_2O_5 is amphoteric. Therefore, it remains challenging and highly desirable to develop a facile and effective strategy to synthesis large-area pure V_2O_5 NSs to achieve excellent lithium storage, cycling, and rate performance.

Herein, we demonstrate a novel and facile dissolution–splitting method to prepare V_2O_5 NSs from its layered crystal, wherein $(NH_4)_2V_6O_{16}$ intercalated compound NSs are first obtained as an intermediate phase and then decomposed into V_2O_5 by calcination. Interestingly, in sharp contrast to its parent bulk crystal, the as-prepared V_2O_5 NSs exhibit greatly enhanced lithium storage properties, including high reversible capacity as well as good cyclic capacity retention and rate performance over a wide temperature range. Furthermore, the low-cost raw materials, commercial V_2O_5 powder and ammonium persulfate (APS), and the facile nature of the experimental procedures favorably enable the proposed method suitable for large-scale fabrication.

Results and Discussion

Figure 1 schematically illustrates the synthetic procedure for the preparation of V_2O_5 NSs. In APS solution, the NH_4^+ ions are first intercalated into the interspace between the layers of bulk V_2O_5 to form intercalated compound $(NH_4)_2V_6O_{16}$. Meanwhile,

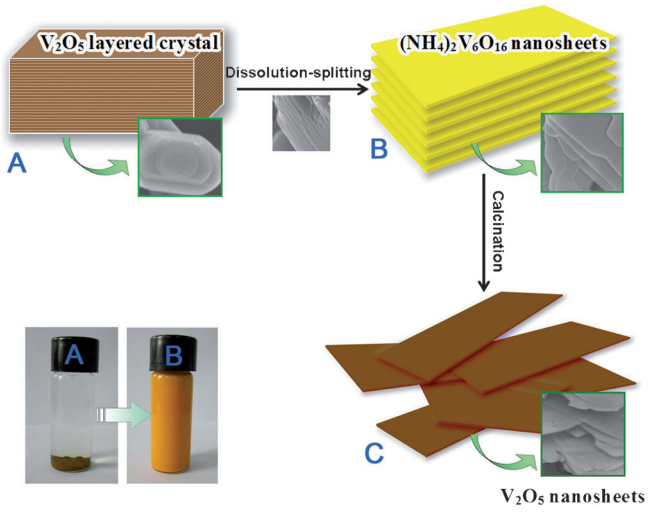

Figure 1. Schematic illustration of the steps for preparation of V_2O_5 nanosheets.

part interlayers of the crystal are dissolved because of the acid environment provided by $S_2O_6^{2-}$, which leads to the peeling of NSs from the parent bulk crystal, that is to say, the splitting process is the dissolving of interlayers. After the dissolution–splitting process occurs, the volume of NSs expands greatly (see Figure S1 in the Supporting Information). The obtained $(NH_4)_2V_6O_{16}$ NSs are dried and then calcinated in air to give V_2O_5 NSs.

The morphology and structure of the prepared samples is compared by scanning electron (SEM) and transmission electron microscopy (TEM). It can be clearly seen that the as-prepared $(NH_4)_2V_6O_{16}$ intercalated compound has a large-area 2D structure (Figure 2A), which is transparent to electrons be-

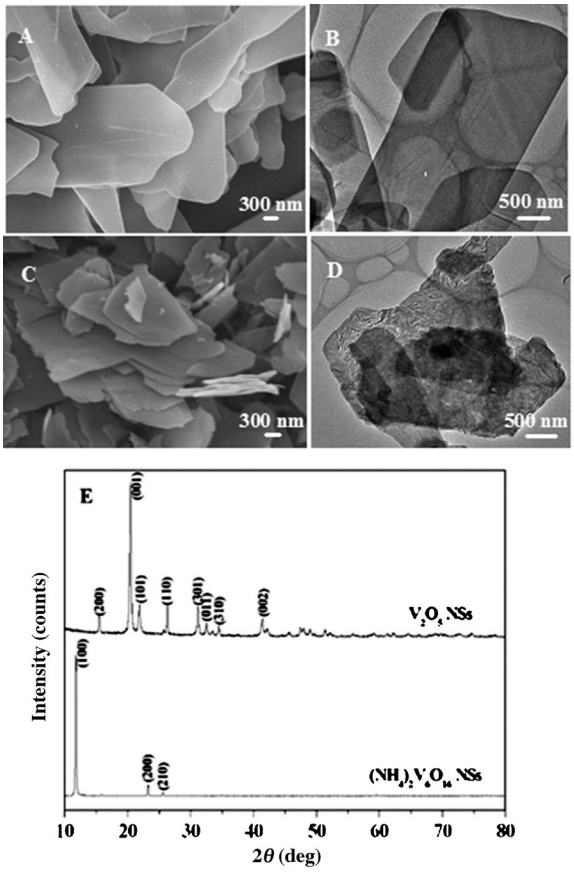

Figure 2. A) SEM image and B) TEM image of $(NH_4)_2V_6O_{16}$ nanosheets. C) SEM image and D) TEM image of V_2O_5 nanosheets. E) XRD patterns of $(NH_4)_2V_6O_{16}$ and V_2O_5 nanosheets.

cause the carbon grid is clearly seen below the nanosheets (Figure 2B). This strongly suggests very thin nanosheets, especially considering the high atomic number of V. The thin nature of the nanosheets was then examined by atomic force microscopy (Figure S2) and shows that such NSs are 10–20 nm in thickness and several micrometers in lateral width, thus indicating that the micrometer-sized 3D layered V_2O_5 crystal (Figure S1A) has been successfully split into thin 2D NSs. Furthermore, our detailed investigation reveals that the reaction time and the concentration of APS play important roles in the for-

mation of such large-area thin sheet structures. The etching of interlayers can be clearly observed even at short reaction times (Figure S3A and S3B), thus demonstrating the dissolution–splitting process. However, if the reaction time is less than 24 hours, bulk crystal or thick sheets can also be observed, thus illustrating that the splitting process is slow and gradual. Interestingly, when the reaction time is further prolonged (Figure S3E and S3F), the thickness of the sheets is not obviously changed but the lateral size becomes smaller, thus implying that layered splitting might turn into lateral splitting. On the other hand, the concentration of APS also affects the degree of splitting (Figure S4) and the characteristics of the sheets (with respect to the concentration of APS) are similar to those observed with varying the reaction time. Figure 2C,D shows the SEM and TEM images of V_2O_5 NSs. After calcination, the shape of the NSs is almost unchanged (Figure 2C), while the surface becomes rough compared to that of $(NH_4)_2V_6O_{16}$ NSs. This change is due to the release of NH_3 and H_2O during decomposition. The high-resolution TEM image (Figure S5) shows that the lattice fringe and the interplanar distance is measured to be 0.44 nm, corresponding to the (001) plane of Shcherbinaite V_2O_5.

The chemical compositions of the samples were studied by X-ray diffraction (XRD). As shown in Figure 2E, the diffraction peaks for the intermediate phase at 2θ of 11.3°, 22.7°, and 25.1° can be indexed to the (100), (200), and (210) planes of $(NH_4)_2V_6O_{16}$ (JCPDS card no. 22-1046), respectively, thus showing that the intercalated compound has been formed. Thermogravimetric analysis was then employed to determine the temperature of $(NH_4)_2V_6O_{16}$ decomposition (Figure S6). It was found that a significant weight loss takes place at 340 °C, and the weight fraction of intercalated molecules is measured to be about 9.3%. After heat treatment at 350 °C for 1 hour, the XRD profile changed significantly and the diffraction peaks at 2θ of 20.3°, 21.7°, 26.3°, and 31.1° can be indexed to the (001), (101), (110), and (301) planes of the Shcherbinaite phase V_2O_5 (JCPDS card no. 65-0131), thus indicating that the intermediate phase was completely transformed into crystalline V_2O_5. The product shows a well-defined crystalline structure and strong (001) diffraction peaks, which suggests that the crystal of NSs is oriented along the (001) direction—this is in good agreement with the above TEM results (Figure S5).

We subsequently investigated the electrochemical properties of these unique V_2O_5 NSs as a cathode material for LIBs. Figure 3A shows the cyclic voltammograms (CVs) of V_2O_5 NSs and bulk V_2O_5 for lithiation/delithiation in the voltage range of 2–4 V. As clearly shown in Figure 3A, each sample exhibits two stages during the electrochemical reaction, one of which is between 4 and 3 V and the other is between 2.7 and 2 V, and correspond to insertion and extraction of the first and second lithium ions, respectively.[28,29] Because of the irreversible structure changes of the $Li_xV_2O_5$ when polarized to 2 V, the reaction process is characterized by four to five sets of CV peaks, part of which may appear as shoulders.[30,31] In comparing the two curves, the distinguish feature is that the peak current density of V_2O_5 NSs is much larger than that of the bulk V_2O_5. It has been reported that if the charge transfer at the interface is fast enough and the rate-limiting step is the lithium diffusion in the electrode, then the peak current is proportional to the contact area between the electrode and electrolyte.[19,32] The nanosheet structure of V_2O_5 intrinsically holds higher contact surface area between electrode material and electrolyte and thus certainly increase the peak current density, which would also benefit their rate performance (see below). Furthermore, the nanosheet structure significantly promotes the electrochemical reactions of V_2O_5 and maintains the crystalline $Li_xV_2O_5$ phases in contrast to the bulk counterpart,[33] and is clearly reflected in

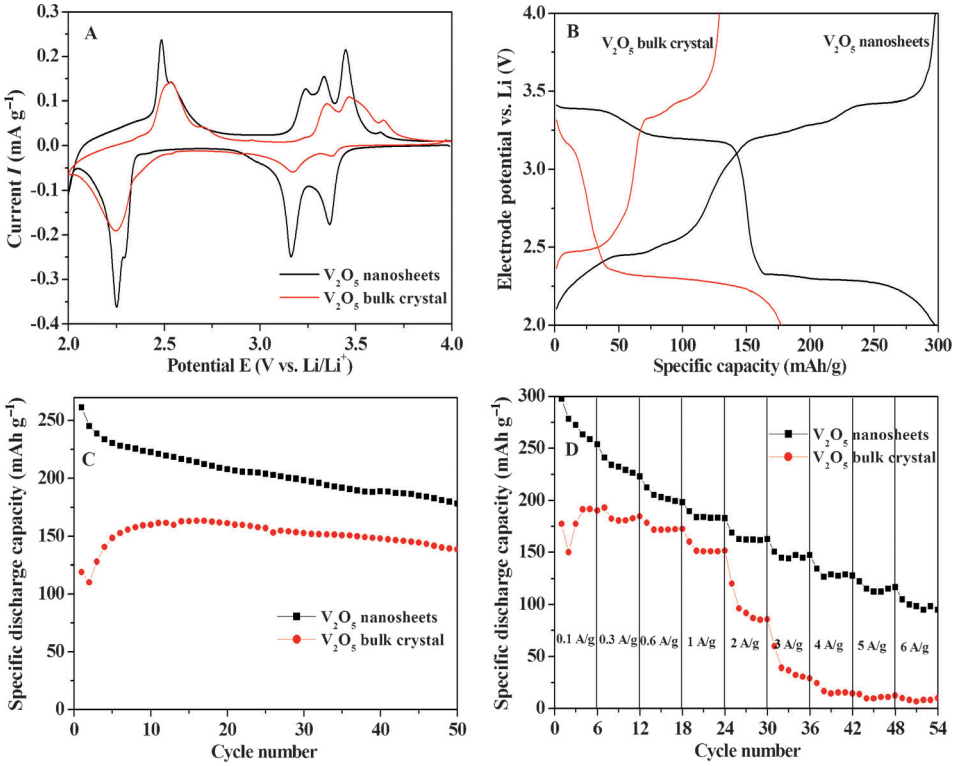

Figure 3. A) CV curves of V_2O_5 nanosheets and bulk crystal in a voltage range of 2–4 V at a scan rate of 0.1 mV s^{-1}. B) Discharge/charge voltage profiles of V_2O_5 nanosheets and bulk crystal at a current density of 100 mA g^{-1}. C) Comparative cycling performance of the two samples at a current density of 300 mA g^{-1}. D) Rate performance at different current densities from 0.1 A g^{-1} to 6 A g^{-1}. All measurements were conducted with a voltage window of 2–4 V.

the CV curves (two more redox peaks are observed in the nanosheet compared to in the bulk).

Figure 3B shows the first cycles for the V_2O_5 NSs and bulk crystal between 2 and 4 V. It can be seen that the discharge/charge plateaus are in good agreement with the CV results. It is clearly observed that the V_2O_5 nanosheet structure exhibits obvious advantage of capacity in comparison with that of the parent bulk crystal. The first specific discharged capacity of NSs is as high as 290 mAh g^{-1} (nearly equal to its theoretic capacity of V_2O_5 with two Li^+ insertion: 294 mAh g^{-1}) at the current density of 100 mA g^{-1} ($\approx$0.3 C), which is much higher than that of the parent bulk crystal (178 mAh g^{-1}). Besides the high capacity, V_2O_5 NSs also exhibit superior cycle stability over the bulk crystal (Figure 3C). After 50 cycles, the discharge capacity of V_2O_5 NSs can still reach 180 mAh g^{-1} at the current of density of 300 mA g^{-1} ($\approx$1 C), meanwhile the bulk crystal only gives 138 mA g^{-1} under the same conditions. Figure 3D demonstrates the rate capability of V_2O_5 NSs and V_2O_5 bulk crystal from current densities of 0.1–6 A g^{-1} for six cycles at each current density. Interestingly, the specific discharge capacities can still remain at 144 and 95 mAh g^{-1} for the V_2O_5 NSs even at the high current density of 3 A g^{-1} ($\approx$10 C) and 6 A g^{-1} ($\approx$20 C), respectively, thus illustrating the outstanding high power and high energy performance of NSs (15.6 kW kg^{-1} and 260 Wh kg^{-1} in Figure S7). This rate capability is much better compared to the results reported in the literature.[29,34] Interestingly, the NSs show excellent cycling stability at the high current density (Figure S8). We can perhaps attribute these greatly enhanced lithium storage properties to the fine nanosheet structure which provides a high interfacial contact area between electrode and electrolyte and a shortened lithium ions diffusion and electron transportation distance, thus leading to the high capacity and high rate performances.

As a battery delivering high power, the Joule effect must be considered because a large amount of heat would be generated during the charge/discharge processes at high power.[35] Meanwhile, the low-temperature performance is also a very important aspect form the view point of practical applications. Therefore, it is of great importance to investigate the temperature-dependent performance of V_2O_5 NSs. Measurements were carried out at −20, 0, 25, and 55 °C. The results are shown in Figure 4 and Figure S8 in the Supporting Information. Interestingly, the rate capabilities are very close at 0, 25, and 55 °C (Figure 4A), thus indicating that the rate performance is not affected by temperature in the range of 0–55 °C. Notably, V_2O_5 NSs also exhibit excellent low-temperature performance including the rate capability, high capacity, and cycling stability. As shown in Figure 4B and Figure S9, at low temperatures of 0 and −20 °C, it could still deliver high capacities of 184 and 158 mAh g^{-1} at a current density of 300 mA g^{-1} ($\approx$1 C) and also exhibit excellent cycling stability.[29,30] Such results are much higher than those reported in the literature (102 and 77.5 mAh g^{-1}).[36,37] This is a very beneficial feature and expands the range of applications of lithium-ion batteries.

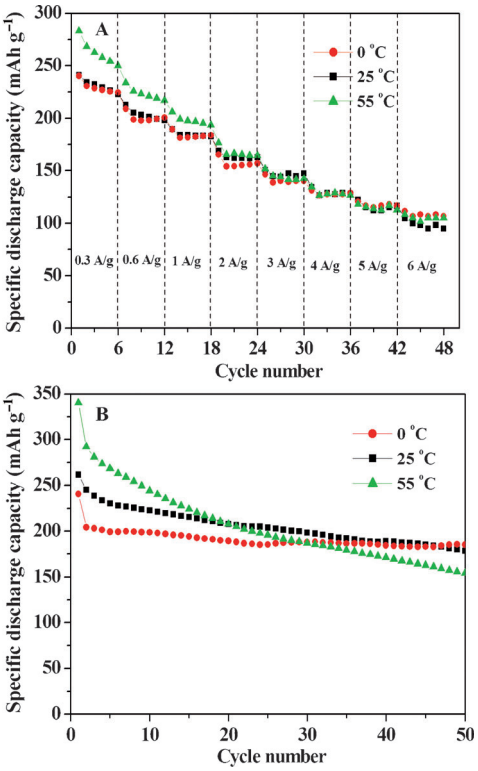

Figure 4. The performance comparisons of V_2O_5 nanosheets at 0, 25, and 55 °C: A) Rate capability and B) cycling at a current density of 300 mA g^{-1}.

Conclusion

In summary, we have developed a facile, low-cost, and effective dissolution–splitting method for the scalable synthesis of large-area pure V_2O_5 nanosheets from their parent bulk crystal. Interestingly, in contrast to the bulk counterpart, the as-prepared V_2O_5 NSs exhibit greatly enhanced lithium storage properties over a wide temperature range. It can deliver a high power density of 15.6 kW kg^{-1} while the energy density remains as high as 260 Wh kg^{-1}, which would bridge the performance gap between batteries and supercapacitors. At low temperatures of 0 and −20 °C, it can still deliver high capacities of 184 and 158 mAh g^{-1} at 1 C and also exhibit good cycling stability, thus highlighting the effectiveness and value of our proposed protocol. The obtained excellent performance opens up new opportunities in the development of high performance next-generation LIBs used for alternative energy and electric transportation. The proposed synthetic strategy may be easily extended to other layered materials which can be used in broad fields including catalysis and sensors.

Experimental Section

Typical synthesis of $(NH_4)_2V_6O_{16}$ nanosheets: Commercial V_2O_5 power (0.36 mg) and APS (4.4 g, 20 mmol) were added to H_2O (36 mL). After the mixture had been stirred for 48 h at 50 °C, the golden-yellow precipitate was collected by centrifugation, washed thoroughly with H_2O, and freeze-dried. The as-prepared $(NH_4)_2V_6O_{16}$

NSs were further treated at 350 °C in air for 1 h with a heating rate of 2 °C min^{-1} to obtain V_2O_5 NSs. To optimize the experimental conditions, different reaction time and concentration of APS were investigated.

Acknowledgements

This study was financially supported by the 100 Talents Programme of The Chinese Academy of Sciences, the National Natural Science Foundation of China (grant no. 21101147), and the Jilin Province Science and Technology Development Program (grant nos. 20100102 and 20116008).

Keywords: batteries · dissolution–splitting method · multielectron reactions · nanosheets · vanadium pentoxide

[1] H. Ma, S. Y. Zhang, W. Q. Ji, Z. L. Tao, J. Chen, *J. Am. Chem. Soc.* **2008**, *130*, 5361 – 5367.
[2] W. Hu, X.-B. Zhang, Y.-L. Cheng, Y.-M. Wu, L.-M. Wang, *Chem. Commun.* **2011**, *47*, 5250 – 5252.
[3] C. Li, L. Gu, S. Tsukimoto, P. A. van Aken, J. Maier, *Adv. Mater.* **2010**, *22*, 3650 – 3654.
[4] B. Kang, G. Ceder, *Nature* **2009**, *458*, 190 – 193.
[5] X. L. Wu, L. Y. Jiang, F. F. Cao, Y. G. Guo, L. J. Wan, *Adv. Mater.* **2009**, *21*, 2710 – 2714.
[6] S. W. Oh, S. T. Myung, Oh, S. M. K. H. Oh, K. Amine, B. Scrosati, Y. K. Sun, *Adv. Mater.* **2010**, *22*, 4842 – 4845.
[7] Z. S. Chao, E. Ruckenstein, *J. Catal.* **2004**, *222*, 17 – 31.
[8] J. F. Liu, X. Wang, Q. Peng, Y. D. Li, *Adv. Mater.* **2005**, *17*, 764 – 767.
[9] T. Y. Zhai, H. M. Liu, H. Q. Li, X. S. Fang, M. Y. Liao, L. Li, H. Y. Zhou, Y. Koide, Y. Bando, D. Golberg, *Adv. Mater.* **2010**, *22*, 2547 – 2552.
[10] M. S. Whittingham, *J. Electrochem. Soc.* **1976**, *123*, 315 – 320.
[11] D. M. Yu, C. G. Chen, S. H. Xie, Y. Y. Liu, K. Park, X. Y. Zhou, Q. F. Zhang, J. Y. Li, G. Z. Cao, *Energy Environ. Sci.* **2011**, *4*, 858 – 861.
[12] N. A. Chernova, M. Roppolo, A. C. Dillon, M. S. Whittingham, *J. Mater. Chem.* **2009**, *19*, 2526 – 2552.
[13] D. W. Liu, G. Z. Cao, *Energy Environ. Sci.* **2010**, *3*, 1218 – 1237.
[14] Y. Wang, K. Takahashi, K. Lee, G. Z. Cao, *Adv. Funct. Mater.* **2006**, *16*, 1133 – 1144.
[15] A. M. Cao, J. S. Hu, H. P. Liang, L. J. Wan, *Angew. Chem.* **2005**, *117*, 4465 – 4469; *Angew. Chem. Int. Ed.* **2005**, *44*, 4391 – 4395.
[16] K. Takahashi, Y. Wang, G. Z. Cao, *Appl. Phys. Lett.* **2005**, *86*, 053102.
[17] K. Takahashi, S. J. Limmer, Y. Wang, G. Z. Cao, *J. Phys. Chem. B* **2004**, *108*, 9795 – 9800.
[18] J. K. Lee, G. P. Kim, I. K. Song, S. H. Baeck, *Electrochem. Commun.* **2009**, *11*, 1571 – 1574.
[19] A. Pan, J.-G. Zhang, Z. M. Nie, G. Z. Cao, B. W. Arey, G. S. Li, S. Q. Liang, J. Liu, *J. Mater. Chem.* **2010**, *20*, 9193 – 9199.
[20] Y. Wang, H. J. Zhang, W. X. Lim, J. Y. Lin, C. C. Wong, *J. Mater. Chem.* **2011**, *21*, 2362 – 2368.
[21] S. J. Ding, D. Y. Luan, F. Y. C. Boey, J. S. Chen, X. W. Lou, *Chem. Commun.* **2011**, *47*, 7155 – 7157.
[22] S. J. Ding, J. S. Chen, D. Y. Luan, F. Y. C. Boey, S. Madhavi, X. W. Lou, *Chem. Commun.* **2011**, *47*, 5780 – 5782.
[23] M. Fang, C. H. Kim, G. B. Saupe, H. N. Kim, C. C. Waraksa, T. Miwa, A. Fujishima, T. E. Mallouk, *Chem. Mater.* **1999**, *11*, 1526 – 1532.
[24] R. Abe, K. Shinohara, A. Tanaka, M. Hara, J. N. Kondo, K. Domen, *J. Mater. Res.* **1998**, *13*, 861 – 865.
[25] T. Sasaki, M. Watanabe, H. Hashizume, H. Yamada, H. Nakazawa, *J. Am. Chem. Soc.* **1996**, *118*, 8329 – 8335.
[26] Z. H. Liu, K. Ooi, H. Kanoh, W. P. Tang, T. Tomida, *Langmuir* **2000**, *16*, 4154 – 4164.
[27] R. Ma, T. Sasaki, *Adv. Mater.* **2010**, *22*, 5082 – 5104.
[28] Y. Omomo, T. Sasaki, L. Z. Wang, M. Watanabe, *J. Am. Chem. Soc.* **2003**, *125*, 3568 – 3575.
[29] L. Q. Mai, L. Xu, C. H. Han, X. Xu, Y. Z. Luo, S. Y. Zhao, Y. L. Zhao, *Nano Lett.* **2010**, *10*, 4750 – 4755.
[30] M. Koltypin, V. Pol, A. Gedanken, D. Aurbach, *J. Electrochem. Soc.* **2007**, *154*, A605 – A613.
[31] A. Odani, V. G. Pol, S. V. Pol, M. Koltypin, A. Gedanken, D. Aurbach, *Adv. Mater.* **2006**, *18*, 1431 – 1436.
[32] X. H. Rui, N. Ding, J. Liu, C. Li, C. H. Chen, *Electrochim. Acta* **2010**, *55*, 2384 – 2390.
[33] M. G. Kim, H. Kim, J. Cho, *J. Electrochem. Soc.* **2010**, *157*, A802 – A807.
[34] Y. S. Hu, X. Liu, J. O. Müller, R. Schlögl, J. Maier, D. S. Su, *Angew. Chem.* **2009**, *121*, 216 – 220; *Angew. Chem. Int. Ed.* **2009**, *48*, 210 – 214.
[35] J. Yan, A. Sumboja, E, Khoo, P. S. Lee, *Adv. Mater.* **2011**, *23*, 746 – 750.
[36] C. R. Sides, C. R. Martin, *Adv. Mater.* **2005**, *17*, 125 – 128.
[37] S. Q. Wang, Z. D. Lu, D. Wang, C. G. Li, C. H. Chen, Y. D. Yin, *J. Mater. Chem.* **2011**, *21*, 6365 – 6369.

Received: November 18, 2011
Published online on January 9, 2012

